ACS APPLIED NANO MATERIALS

Open Access

www.acsanm.org

Article

Gas Phase Photocatalysis on Large-Scale TiO_2 Nanotube Layers for Pollutant Degradation: Influence of the Nanotube Crystallinity

Hanna Sopha, Michal Baudys, Marcela Sepúlveda, Jakub Rusek, Ludek Hromadko, Jhonatan Rodriguez-Pereira, Josef Krysa, and Jan M. Macak*

Cite This: *ACS Appl. Nano Mater.* 2023, 6, 17053−17059

Read Online

ACCESS | Metrics & More | Article Recommendations | Supporting Information

ABSTRACT: In this work, for the first time, the influence of the crystallinity of TiO_2 nanotube (TNT) layers on their gas phase photocatalytic performance was investigated under ISO standards using two distinct model pollutants, namely, hexane and acetaldehyde. TNT layers (1 μm thick) on 5 × 10 cm^2 large Ti substrates were employed in this work due to their excellent adhesion to Ti upon annealing at high temperatures. Annealing of the TNT layers was carried out in a temperature range between 300 and 700 °C, resulting in TNT layers with different crystallinities, i.e., from the pure anatase phase to an 85% rutile phase. The superior performance of the TNT layers annealed at 600 °C with mixed anatase and rutile phase compared to other specimens was observed for both model pollutants, stemming from the band alignment between the two crystalline phases. For higher annealing temperatures, however, the photocatalytic performance of the TNT layers was reduced due to a partial disintegration of the TNTs. No surface contamination of the TNT layers with residues of pollutant degradation products was observed after experiments.

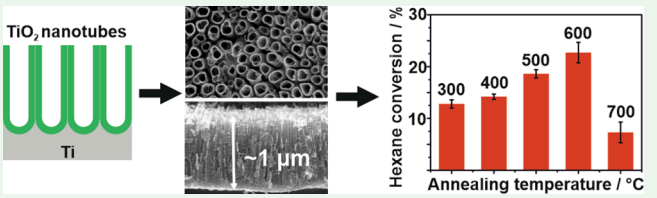

KEYWORDS: *gas phase photocatalysis, TiO_2 nanotube layers, annealing temperature, crystallinity, pollutants, VOCs*

INTRODUCTION

Air pollution is one of the major environmental problems. Volatile organic compounds (VOCs), exposed by many urban and industrial sources into the air, are harmful to humans and the environment and should therefore be removed from air. The optimal recovery or degradation method is dependent on the VOC concentration.[1−3] For low, indoor pollution levels in the ppb or low ppm range, photocatalysis can be the method of choice for VOC degradation[4−6] as it leads to the degradation of pollutants to nonharmful compounds under ambient conditions, ideally up to their complete mineralization to CO_2 and water.[7]

Semiconducting TiO_2 is known as an excellent photocatalyst, which shows a high stability and nontoxicity in addition to a high photocatalytic performance. Upon UV light illumination, electron−hole pairs are formed within the TiO_2, leading to the formation of radicals with high oxidative power, which in turn can oxidize gaseous or liquid organic pollutants.[2,8,9] UV light irradiation is required for this process due to high bandgaps of 3.2 eV for the anatase phase and 3.0 eV for the rutile phase TiO_2.[10−13]

For efficient pollutant degradation, photocatalysts with a large surface area are advantageous. Therefore, often nanostructured photocatalysts are used in the literature as, e.g., nanoparticles, nanorods, or nanotubes.[3,14−19] Within the last ~15 years, specifically, TiO_2 nanotube (TNT) layers, prepared by anodic oxidation of Ti,[20,21] have gained paramount attention as photocatalysts due to their outstanding performance. Thus, compared to benchmark P25 nanoparticles, TNT layers have shown a higher photocatalytic performance in the liquid as well as in the gas phase.[17,22] This can be explained by the fact that anodic TNT layers grow in a highly ordered manner with a vertical alignment during electrochemical anodization, with the nanotube openings toward the top of the layers, while the closed nanotube bottoms are attached to the Ti substrate.[20,21] Thus, the TNT layers naturally have a very high available surface area and show a straight diffusion way and an improved charge separation stemming from the unidirectional dimensionality of the nanotubes.[17,23] Additionally, compared to other nanostructures, they have the advantage that they are attached to a substrate without any further immobilization necessary and can easily be removed from a photocatalytic reactor. On the other hand, if free nanotubes are required, then they can be removed from the Ti substrate by bending the substrate or by etching to receive nanotube bundles or single nanotubes.[24−26] It must be pointed out that the as-prepared TNT layers are amorphous. However, they can be converted into the anatase phase or a mixture

Received: July 12, 2023
Accepted: September 1, 2023
Published: September 12, 2023

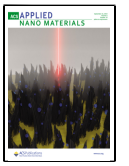

between the anatase and rutile phase by annealing at temperatures between ~350 and ~700 °C.[27−29]

In the literature, many studies can be found on using TNT layers for photocatalytic applications; however, most of them report on liquid phase photocatalysis,[17,18,21] while comparably few publications investigate the applicability of TNT layers for gas phase photocatalysis.[30−33] Moreover, most studies were carried out on the lab scale, meaning the TNT layers were prepared on rather small Ti substrates with areas of up to ~10 cm^2, while only a few studies were carried out on larger substrates.[22,32,34−40] The reason for this is probably the difficulty in anodization of large Ti substrates as high currents are flowing between the Ti substrate and the counter electrode, heating up the electrolyte with high possibility of the dielectric breakdown occurrence.[32,41] However, for possible real applications, TNT layers on larger areas are necessary. Recently, we have shown the anodization of Ti foils toward homogeneous TNT layers of different thicknesses on an area of 100 cm^2.[32] Such larger TNT layers can be employed in photocatalytic gas phase reactors under ISO standards. In the mentioned study,[32] the as-prepared amorphous TNT layers were annealed at 400 °C to receive the anatase phase. However, several studies on the influence of the annealing temperature of small TNT layers for photocatalytic degradation of pollutants in the liquid phase can be found in the literature.[42−48] The results of these studies are not unambiguous. While some studies claim that the pure anatase phase shows the best results for the photocatalytic degradation of the used pollutants,[43−47] other studies show an improved performance when the TNT layers were composed of a mixture of anatase and rutile.[42,48] A reason for this can be that at higher temperatures, when rutile begins to form, TNT layers often start to sinter and disintegrate, resulting in thicker nanotube walls and a reduction in TNT layer thickness and consequently in a decrease in surface area.[43]

To the best of our knowledge, no studies on the influence of the TNT crystalline structure (driven by the annealing temperature of TNT layers) on the photocatalytic performance in the gas phase can be found in the current literature. However, in view of possible real applications of the TNT layers for photocatalytic degradation of gaseous compounds, such studies should also be carried out for the gas phase. In this study, photocatalysis with two common VOCs, namely, hexane and acetaldehyde, was carried out on 1 μm-thick TNT layers produced on an area of 50 cm^2 under ISO standards (ISO 22197). The relatively thin TNT layers were chosen for three reasons: (i) it is known that these TNT layers can be annealed to at least 600 °C without any obvious disintegration or lifting off of the TNT layers,[49] (ii) as the rutile phase starts to grow from the underlying Ti substrate, already small amounts of the rutile phase are traceable,[27,49] and (iii) such thin TNT layers are relatively easy to prepare also on the large scale without the risk of dielectric breakdown.[32]

EXPERIMENTAL SECTION

TiO_2 nanotube (TNT) layers were produced in a two-electrode setup using Ti foil (5 × 12 cm^2, Sigma-Aldrich, 0.127 mm thick) as the anode and a Ti foil of the same size (Sigma-Aldrich, 0.250 mm thick) as the cathode. The Ti foil was anodized on an area of 5 × 10 cm^2 in a glycerol-based electrolyte containing 270 mM NH_4F and 50 vol % H_2O at 20 V (PGU-200 V, IPS Elektroniklabor GmbH) for 100 min under mild cooling conditions to 16 °C to receive 1 μm-thick TNT layers with a nanotube diameter of ~80 nm.[32] After anodization, the TNT layers were rinsed and sonicated in isopropyl alcohol to remove the electrolyte. Before further use, the amorphous TNT layers were annealed in a muffle oven at five different temperatures, namely, 300, 400, 500, 600, and 700 °C to convert the amorphous into crystalline TiO_2. The time needed to heat the oven to the final temperature was kept constant at 3 h. Scheme 1 illustrates the TNT layer preparation.

Scheme 1. Schematic Illustration of the TNT Layer Preparation

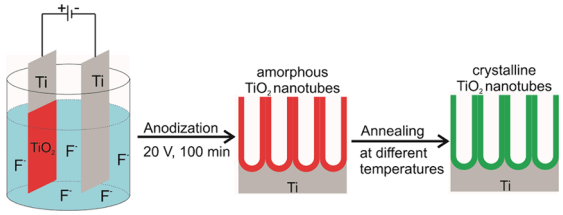

Photocatalytic degradation experiments were carried out for two gaseous compounds, i.e., hexane and acetaldehyde, in a photoreactor built according to ISO standards (ISO 22197) with a photocatalyst area of 50 cm^2. A scheme of the reactor is given in our previous publications.[22,32] In brief, a calibrated gas mixture of 100 ppm of hexane or acetaldehyde in N_2 (Linde Gas) was used as a pollutant source. A final concentration of 5 ppm of the respective pollutant was reached by the dilution of the calibrated gas with humidified air, which was flown through the reactor with flow rates of 1 and also 2 L/min (in the case of acetaldehyde). The relative humidity (RH) in the reactor was set to 50%, in line with the ISO standards. The gas mixture was analyzed using a gas chromatograph equipped with a flame ionization detector (GC 7890B (Agilent) with a capillary column (HP Plot U (15 × 0.25) Agilent). All photocatalytic degradation tests were carried out twice on two different TNT layers for statistical evaluation.

The surface morphology of the TNT layers was characterized using field-emission scanning electron microscopy (FE-SEM, JEOL JSM 7500F), and proprietary Nanomeasure software was employed for the evaluation of the nanotube dimensions, i.e., nanotube diameter and nanotube layer thickness. As the TNT layers were cut for cross-sectional SEM analyses, different TNT layers had to be used for the morphological investigation of unused and used (after photocatalytic experiments) TNT layers. X-ray diffraction (XRD, Panalytical Empyrean, equipped with a Cu X-ray tube and a Pixcel 3D scintillation detector) was employed to study the crystallinity of the TNT layers annealed at different temperatures. The measurements were carried out at 45 kV. X-ray photoelectron spectroscopy (XPS, ESCA2SR, Scienta-Omicron) with a monochromatic Al Kα (1486.7 eV) X-ray source was carried out to acquire the surface composition of the TNT layers. The binding energy scale was referenced to adventitious carbon (284.8 eV), while quantitative analysis was performed by using CasaXPS software with the elemental sensitivity factors provided by the manufacturer.

RESULTS AND DISCUSSION

Figure 1 shows XRD patterns of the TNT layers annealed at different temperatures. As one can see, the TNT layers annealed at 300 and 400 °C reveal purely anatase TiO_2 peaks (ICSD: 154603) and Ti peaks (ICSD: 653280), stemming from the underlying Ti substrate. After annealing of the TNT layer at 500 °C, additionally, a small rutile TiO_2 peak (ICSD: 169622) at 2θ ~27.4° was observed, indicating the initiation of the anatase-to-rutile transformation. This rutile diffraction peak increased in intensity when the annealing temperature was further increased to 600 and 700 °C. At the same time, more diffraction peaks of the rutile phase appeared, while the anatase peak decreased in intensity. This indicates that more rutile was formed by transformation of the anatase phase. Moreover, the intensity of the Ti peaks from the underlying Ti substrates

https://doi.org/10.1021/acsanm.3c03199
ACS Appl. Nano Mater. 2023, 6, 17053−17059

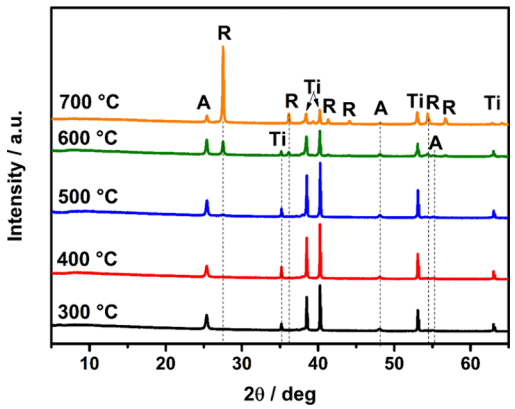

Figure 1. XRD patterns of the TNT layers annealed at different temperatures. A, anatase; R, rutile; Ti, titanium.

decreased, suggesting the formation of a thicker oxide layer between the TNT layers and the Ti substrate. The growth of such oxide layers, with the rutile phase growth starting from this layer, is known from the literature and is detrimental for electrochemical applications due to a reduction in electron mobility and thus in conductivity of the TNT layers.[49] However, such an oxide layer should not decrease the photocatalytic efficiency when no electrical contact needs to be established, which is the present case.

Crystallite sizes, calculated using the Scherrer equation, and weight fractions of the anatase and rutile phase within the TNT layers are given in Table 1. The overall anatase and rutile crystallite sizes increased with the temperature, which is in line with the literature.[27−29,50]

Table 1. Crystallite Sizes and Weight Fractions for Anatase and Rutile Phases of TNT Layers Annealed at Different Temperatures

	crystallite size/nm		weight fraction/%	
annealing temperature/°C	anatase	rutile	anatase	rutile
300	29.7		100	0
400	30.4		100	0
500	33.7	12.4	95.8	4.2
600	36.3	39.5	57.2	42.8
700	37.9	54.5	15.4	84.6

The weight fraction of rutile was found very low with 4.2% after annealing of the TNT layers at 500 °C. However, for an annealing temperature of 600 °C, the weight fractions of anatase and rutile are almost equal, while after annealing at 700 °C, a weight fraction of rutile of almost 85% was found. This means that by variation of the annealing temperature, TNT layers with very different structures were prepared.

To investigate the surface morphology of the TNT layers annealed at different temperatures, SEM analyses were carried out. Figure 2 shows the top view and cross-sectional SEM images of the TNT layers annealed at different temperatures. The top views, shown in the left column, reveal no significant differences for annealing temperatures between 300 and 600 °C. However, after annealing at 700 °C, the nanotube walls seem to be more rounded indicating the beginning of a melting or sintering of the nanotubes. Statistical evaluations of the nanotube diameters and wall thicknesses are given in Table 2. The average nanotube diameter is in the same range for all

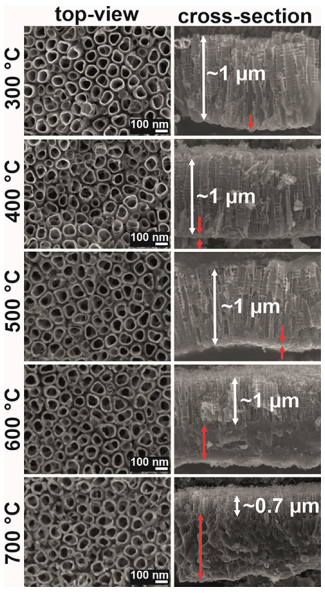

Figure 2. SEM top views (left column) and cross-sectional views (right column) of TNT layers annealed at different temperatures. The red arrows indicate the thermal TiO_2 layer grown between the TNT layers and the Ti substrate due to the annealing.

Table 2. Average Nanotube Diameter and Wall Thickness of TNT Layers Annealed at Different Temperatures

annealing temperature/°C	nanotube diameter/nm	wall thickness/nm
300	77 ± 13	8 ± 2
400	73 ± 12	9 ± 2
500	74 ± 12	11 ± 2
600	78 ± 12	13 ± 3
700	74 ± 12	15 ± 4

TNT layers annealed at different temperatures. However, the wall thickness of the TNT layers, measured on the nanotube tops, increases from ∼8.5 to ∼15 nm for TNT layers annealed at 300 and 700 °C, respectively. While the wall thickness for TNT layers annealed at 300, 400, and 500 °C increased just marginally, a larger increase was observed when the annealing temperature rose from 500 to 600 °C. This can be seen in the SEM images by more rounded nanotube tops. However, the TNT layers did not disintegrate yet, as confirmed by the SEM cross-sectional views, shown in the right column of Figure 2. All TNT layers annealed at temperatures up to 600 °C showed a thickness of ∼1 μm. Nonetheless, after annealing at 700 °C, a sudden decrease in TNT layer thickness to ∼0.7 μm for TNT layers was observed, proving the partial melting and disintegration of the TNT layers annealed at such high temperatures. The partial disintegration of the TNT layers annealed at 700 °C has a negative effect on the photocatalytic performance, as discussed in the corresponding text later on. Additionally, a thermal oxide layer can be observed for TNT layers annealed at all temperatures, as indicated by red arrows. This thermal oxide layer is very thin for TNT layers annealed at 300 °C and thickens with the annealing temperature. This is in accordance with the significant decrease in the Ti peak intensity, as observed in Figure 1 for TNT layers annealed at 600 and 700 °C.

The photocatalytic conversion of the model pollutants, hexane and acetaldehyde, on the TNT layers with different crystallinities after annealing at different temperatures is shown

https://doi.org/10.1021/acsanm.3c03199
ACS Appl. Nano Mater. 2023, 6, 17053−17059

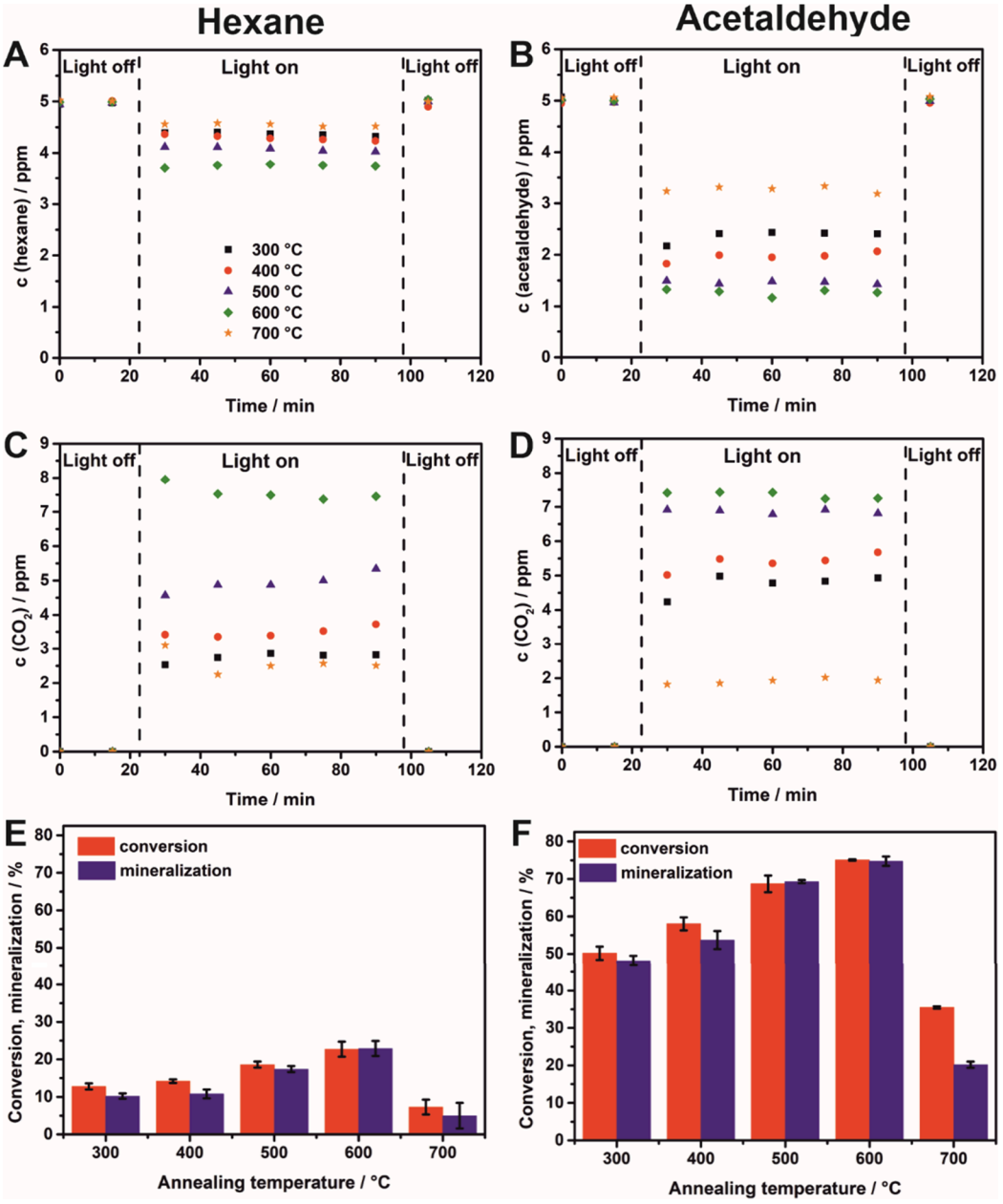

Figure 3. Changes in hexane (A) and acetaldehyde (B) concentrations, CO_2 production upon degradation of hexane (C) and acetaldehyde (D), and conversion and mineralization of hexane (E) and acetaldehyde (F). The legend in panel (A) is also valid for panels (B–D).

in Figure 3. For both pollutants, an increase in the photocatalytic conversion was observed for TNT layers annealed at temperatures up to 600 °C. This increase in photocatalytic conversion can be explained for annealing temperatures of ~300–500 °C, i.e., when mainly the pure anatase phase or very small weight fractions of the rutile phase were observed by an increase in crystallinity and larger crystallite sizes and a decrease in surface states. This is in accordance with the literature on photocatalytic degradation of pollutants on TNT layers in the liquid phase.[43,44]

Additionally, after annealing of the TNT layers at 600 °C, the weight fraction of rutile in the TNT layers rose significantly to a ratio between the anatase and rutile phases of approximately 1:1. Although, as discussed in the Introduction, many studies on the application of TNT layers for photocatalysis in the liquid phase report on the highest performance for TNT layers consisting of the pure anatase phase, it is commonly agreed in the literature that the best photocatalytic efficiency of TiO_2 is achieved, when a mixture of both crystalline phases is used, instead of just one pure crystalline phase.[51−53] This is explained with a synergistic effect ascribed to an integrated driving force for photogenerated charge separation.[54] Several studies[53,55,56] show an energy band alignment of rutile when in contact with anatase, with the conduction and valence band of rutile being of higher energy than those of anatase. Besides the positive effect of the heterojunction on the photocatalytic performance, there seems to be also a positive effect of the underlying rutile layer (due to the increased light absorption) formed by thermal oxidation of Ti. The recent work of Sepúlveda et al.[57] shows that the double-/single-wall nanotubes are still purely anatase after annealing at 600 °C if they are annealed without the Ti

https://doi.org/10.1021/acsanm.3c03199
ACS Appl. Nano Mater. 2023, 6, 17053−17059

substrate underneath. This supports the explanation that the improvement is due to the formation of a rutile layer and improved light absorption and results in significantly higher production of photogenerated charges. The formed heterojunction plays a minor role.

As a result, the TNT layers annealed at 600 °C, revealing a high amount of rutile phase with a weight fraction of 42.8%, show the best photocatalytic performance of the TNT layers employed in this study.

An annealing temperature of 700 °C resulted in a majority of the rutile phase of ∼85% in combination with a partial disintegration of the TNT layers, leading additionally to a significantly decreased available surface area. Therefore, the photocatalytic conversion of the TNT layers decreased upon annealing at higher temperatures.

When comparing the conversion of both model pollutants, it is obvious that an approximately 3 times higher conversion was obtained for acetaldehyde, i.e., the conversions of acetaldehyde and hexane were ∼75 and ∼23%, respectively. This can be attributed to the easier degradation of acetaldehyde compared to hexane, stemming on the one hand from the presence of the reactive carbonyl group in acetaldehyde and on the other hand from the higher solubility of acetaldehyde in water, resulting in a higher affinity of acetaldehyde to the hydrophilic TNT layers compared to the nonpolar hexane.[58] At such high conversions of acetaldehyde, depletion of acetaldehyde in the vicinity of the TNT layers may occur, and the rate of photocatalytic reaction can be limited by mass transfer. For this reason, degradations were repeated at a higher flow rate (2 L/min). The results show that the photocatalytic conversion of acetaldehyde was not limited by the mass transport, and the observed differences in the conversions are due to the differences in crystallinity of the TNT layers annealed at different temperatures.

Additionally to the conversion of both pollutants on the differently annealed TNT layers, mineralization of the pollutants to CO_2 was also measured, which is also shown in Figure 3. Except for the TNT layers annealed at 500 and 600 °C, the mineralization of both pollutants is somewhat lower than the conversion. This means that some hexane and acetaldehyde molecules were not completely decomposed to CO_2 but to some (undesired) intermediates only. However, in the case of the TNT layers annealed at 600 °C, the conversion and mineralization were measured to almost the same percentage, independently of the pollutant, confirming the good performance of these TNT layers.

SEM investigation was carried out on all TNT layers after photocatalytic experiments, as shown in Figure S1. No differences in morphology of the TNT layers were observed compared to the unused TNT layers in Figure 2. This shows that the photocatalytic degradation of the employed pollutants is nondestructive to the TNT layers. To gain more insights into possible contamination or poisoning of the TNT layers with just partly degraded pollutants or other possible contaminants, stemming from the reaction environment, a thorough XPS analysis was carried out on the surface of the TNT layers before and after the photocatalytic tests. Table 3 shows the surface composition of the TNT layers annealed at different temperatures before and after their tests. The survey spectra of the O 1s, Ti 2p, N 1s, and C 1s can be found in Figures S2 and S3. No significant increase in the carbon content on the TNT layer surface or the presence of any other contaminations was observed after the tests, indicating that no contamination or poisoning of the TNT layer surface took place. The relatively small difference in the carbon content observed can be attributed to adventitious carbon.

Table 3. XPS Surface Composition of the Differently Annealed TNT Layers before and after Photocatalytic Tests

		atomic concentration/%			
	annealing temperature/°C	C	O	Ti	N
before photocatalytic tests	300	17.45	58.57	23.25	0.73
	400	16.88	58.96	23.44	0.72
	500	16.29	59.41	23.76	0.55
	600	16.27	59.17	23.95	0.61
	700	15.09	59.88	24.36	0.67
after photocatalytic tests	300	15.90	59.11	23.82	1.16
	400	15.04	59.92	24.11	0.92
	500	14.09	60.44	24.66	0.81
	600	13.62	60.71	24.82	0.85
	700	13.42	61.51	24.33	0.74

CONCLUSIONS

In conclusion, this study shows for the first time the influence of the crystalline structure on the photocatalytic performance of TNT layers in the gas phase for two distinct model pollutants under the ISO standards. It is shown that the best photocatalytic performance of the TNT layers was observed for the mixed crystalline phase consisting of anatase and rutile phases due to a band alignment of the two crystalline phases resulting in an improved charge separation, compared to the pure crystalline phases. Furthermore, when very high annealing temperatures were employed (i.e., 700 °C), the TNT layers start to disintegrate and a consequential decrease in surface area leads to a decrease in photocatalytic performance. It must be noted here that the exact temperatures at which the anatase-to-rutile transformation and a disintegration of the TNT layers start might depend on the dimensions of the TNT layers, i.e., their layer and wall thickness. Therefore, the exact optimal annealing temperatures should always be investigated for the TNT layers employed.

ASSOCIATED CONTENT

Supporting Information

The Supporting Information is available free of charge at https://pubs.acs.org/doi/10.1021/acsanm.3c03199.

SEM investigations after photocatalytic tests and XPS spectra of TNT layers annealed at different temperatures before and after photocatalytic tests (PDF)

AUTHOR INFORMATION

Corresponding Author

Jan M. Macak − *Center of Materials and Nanotechnologies, Faculty of Chemical Technology, University of Pardubice, 53002 Pardubice, Czech Republic; Central European Institute of Technology, Brno University of Technology, 612 00 Brno, Czech Republic;* orcid.org/0000-0001-7091-3022; Email: jan.macak@upce.cz

Authors

Hanna Sopha − *Center of Materials and Nanotechnologies, Faculty of Chemical Technology, University of Pardubice, 53002 Pardubice, Czech Republic; Central European Institute of Technology, Brno University of Technology, 612*

https://doi.org/10.1021/acsanm.3c03199
ACS Appl. Nano Mater. 2023, 6, 17053−17059

00 Brno, Czech Republic; orcid.org/0000-0001-7144-5427

Michal Baudys − *Department of Inorganic Technology, University of Chemistry and Technology Prague, 166 28 Prague, Czech Republic*

Marcela Sepúlveda − *Center of Materials and Nanotechnologies, Faculty of Chemical Technology, University of Pardubice, 53002 Pardubice, Czech Republic;* orcid.org/0000-0003-1847-9040

Jakub Rusek − *Department of Inorganic Technology, University of Chemistry and Technology Prague, 166 28 Prague, Czech Republic*

Ludek Hromadko − *Center of Materials and Nanotechnologies, Faculty of Chemical Technology, University of Pardubice, 53002 Pardubice, Czech Republic; Central European Institute of Technology, Brno University of Technology, 612 00 Brno, Czech Republic*

Jhonatan Rodriguez-Pereira − *Center of Materials and Nanotechnologies, Faculty of Chemical Technology, University of Pardubice, 53002 Pardubice, Czech Republic; Central European Institute of Technology, Brno University of Technology, 612 00 Brno, Czech Republic;* orcid.org/0000-0001-6501-9536

Josef Krysa − *Department of Inorganic Technology, University of Chemistry and Technology Prague, 166 28 Prague, Czech Republic*

Complete contact information is available at: https://pubs.acs.org/10.1021/acsanm.3c03199

Author Contributions

H.S.: conceptualization, data curation, formal analysis, investigation, methodology, writing−original draft, and writing−review and editing. M.B. and J.R.-P.: data curation, formal analysis, investigation, and writing−review and editing. M.S. and J.R.: investigation and writing−review and editing. L.H.: formal analysis visualization and writing−review and editing. J.K. and J.M.M.: conceptualization, methodology, funding acquisition, project administration, supervision, and writing−review and editing. The manuscript was written through the contributions of all authors. All authors have given approval to the final version of the manuscript.

Notes

The authors declare no competing financial interest.

■ ACKNOWLEDGMENTS

The authors acknowledge the Czech Science Foundation (project 21-27243S) and the Ministry of Education, Youth and Sports of the Czech Republic (MEYS CR, project LM2023037).

■ REFERENCES

(1) Dunn, R. F.; El-Halwagi, M. M. Selection of Optimal VOC-Condensation Systems. *Waste Manage.* **1994**, *14* (2), 103−113.

(2) Moulis, F.; Krýsa, J. Photocatalytic Degradation of Several VOCs (n-Hexane, n-Butyl Acetate and Toluene) on TiO_2 Layer in a Closed-Loop Reactor. *Catal. Today* **2013**, *209*, 153−158.

(3) Moulis, F.; Krýsa, J. Photocatalytic Degradation of Acetone and Methanol in a Flow-through photoreactor with Immobilized TiO_2. *Res. Chem. Intermed.* **2015**, *41* (12), 9233−9242.

(4) Jo, W.-K.; Park, K.-H. Heterogeneous Photocatalysis of Aromatic and Chlorinated Volatile Organic Compounds (VOCs) for Non-Occupational Indoor Air Application. *Chemosphere* **2004**, *57* (7), 555−565.

(5) Ao, C. H.; Lee, S. C.; Mak, C. L.; Chan, L. Y. Photodegradation of Volatile Organic Compounds (VOCs) and NO for Indoor Air Purification Using TiO_2: Promotion versus Inhibition Effect of NO. *Appl. Catal., B* **2003**, *42* (2), 119−129.

(6) Ao, C.; Lee, S. Combination Effect of Activated Carbon with TiO_2 for the Photodegradation of Binary Pollutants at Typical Indoor Air Level. *J. Photochem. Photobiol., A* **2004**, *161* (2−3), 131−140.

(7) Fujishima, A.; Zhang, X.; Tryk, D. A. TiO_2 Photocatalysis and Related Surface Phenomena. *Surf. Sci. Rep.* **2008**, *63* (12), 515−582.

(8) Kontos, A. G.; Katsanaki, A.; Maggos, T.; Likodimos, V.; Ghicov, A.; Kim, D.; Kunze, J.; Vasilakos, C.; Schmuki, P.; Falaras, P. Photocatalytic Degradation of Gas Pollutants on Self-Assembled Titania Nanotubes. *Chem. Phys. Lett.* **2010**, *490* (1−3), 58−62.

(9) Sopha, H.; Krbal, M.; Ng, S.; Prikryl, J.; Zazpe, R.; Yam, F. K.; Macak, J. M. Highly Efficient Photoelectrochemical and Photocatalytic Anodic TiO_2 Nanotube Layers with Additional TiO_2 Coating. *Appl. Mater. Today* **2017**, *9*, 104−110.

(10) Hoffmann, M. R.; Martin, S. T.; Choi, W.; Bahnemann, D. W. Environmental Applications of Semiconductor Photocatalysis. *Chem. Rev.* **1995**, *95* (1), 69−96.

(11) Fujishima, A.; Rao, T. N.; Tryk, D. A. Titanium Dioxide Photocatalysis. *J. Photochem. Photobiol., C* **2000**, *1* (1), 1−21.

(12) Tryk, D.; Fujishima, A.; Honda, K. Recent Topics in Photoelectrochemistry: Achievements and Future Prospects. *Electrochim. Acta* **2000**, *45* (15−16), 2363−2376.

(13) Carp, O.; Huisman, C. L.; A, R. Photoinduced Reactivity of Titanium Dioxide. *Prog. Solid State Chem.* **2004**, *32* (1−2), 33−177.

(14) Boulamanti, A. K.; Philippopoulos, C. J. Photocatalytic Degradation of C5-C7 alkanes in the Gas-Phase. *Atmos. Environ.* **2009**, *43* (20), 3168−3174.

(15) Kandiel, T. A.; Feldhoff, A.; Robben, L.; Dillert, R.; Bahnemann, D. W. Tailored Titanium Dioxide Nanomaterials: Anatase Nanoparticles and Brookite Nanorods as Highly Active photocatalysts. *Chem. Mater.* **2010**, *22* (6), 2050−2060.

(16) Lafjah, M.; Mayoufi, A.; Schaal, E.; Djafri, F.; Bengueddach, A.; Keller, N.; Keller, V. TiO_2 Nanorods for Gas Phase Photocatalytic Applications. *Catal. Today* **2014**, *235*, 193−200.

(17) Macak, J. M.; Zlamal, M.; Krysa, J.; Schmuki, P. Self-Organized TiO_2 Nanotube Layers as Highly Efficient photocatalysts. *Small* **2007**, *3* (2), 300−304.

(18) Zlamal, M.; Macak, J. M.; Schmuki, P.; Krysa, J. Electrochemically Assisted Photocatalysis on Self-Organized TiO_2 Nanotubes. *Electrochem. commun.* **2007**, *9* (12), 2822−2826.

(19) Wu, Z.; Dong, F.; Zhao, W.; Wang, H.; Liu, Y.; Guan, B. The Fabrication and Characterization of Novel Carbon Doped TiO_2 Nanotubes, Nanowires and Nanorods with High Visible Light Photocatalytic Activity. *Nanotechnology* **2009**, *20* (23), No. 235701.

(20) Macak, J. M.; Tsuchiya, H.; Ghicov, A.; Yasuda, K.; Hahn, R.; Bauer, S.; Schmuki, P. TiO_2 Nanotubes: Self-Organized Electrochemical Formation, Properties and Applications. *Curr. Opin. Solid State Mater. Sci.* **2007**, *11* (1−2), 3−18.

(21) Lee, K.; Mazare, A.; Schmuki, P. One-Dimensional Titanium Dioxide Nanomaterials: Nanotubes. *Chem. Rev.* **2014**, *114* (19), 9385−9454.

(22) Sopha, H.; Baudys, M.; Krbal, M.; Zazpe, R.; Prikryl, J.; Krysa, J.; Macak, J. M. Scaling up Anodic TiO_2 Nanotube Layers for Gas Phase Photocatalysis. *Electrochem. Commun.* **2018**, *97* (October), 91−95.

(23) Thavasi, V.; Renugopalakrishnan, V.; Jose, R.; Ramakrishna, S. Controlled Electron Injection and Transport at Materials Interfaces in Dye Sensitized Solar Cells. *Mater. Sci. Eng., R* **2009**, *63* (3), 81−99.

(24) Villa, K.; Sopha, H.; Zelenka, J.; Motola, M.; Dekanovsky, L.; Beketova, D. C.; Macak, J. M.; Ruml, T.; Pumera, M. Enzyme-photocatalyst Tandem Microrobot Powered by Urea for Escherichia Coli Biofilm Eradication. *Small* **2022**, *18*, 2106612.

(25) Beketova, D.; Motola, M.; Sopha, H.; Michalicka, J.; Cicmancova, V.; Dvorak, F.; Hromadko, L.; Frumarova, B.; Stoica, M.; Macak, J. M. One-Step Decoration of TiO_2 Nanotubes with

Fe_3O_4 Nanoparticles: Synthesis and Photocatalytic and Magnetic Properties. *ACS Appl. Nano Mater.* **2020**, *3* (2), 1553−1563.
(26) Sepúlveda, M.; Castaño, J. G.; Echeverría, F.; Aoki, Y.; Kowalsk, D.; Habazaki, H. Formation of Quasi-Spherical Au48−198 Clusters in Anodic Titania Nanotubes Grown on Ti-Au Alloys. *Electrochem. Commun.* **2020**, *120* (September), No. 106847.
(27) Varghese, O. K.; Gong, D.; Paulose, M.; Grimes, C. A.; Dickey, E. C. Crystallization and High-Temperature Structural Stability of Titanium Oxide Nanotube Arrays. *J. Mater. Res.* **2003**, *18* (1), 156−165.
(28) Ghicov, A.; Tsuchiya, H.; Macak, J. M.; Schmuki, P. Annealing Effects on the Photoresponse of TiO_2 Nanotubes. *Phys. Status Solidi Appl. Mater. Sci.* **2006**, *203* (4), 28−30.
(29) Sopha, H.; Spotz, Z.; Sepúlveda, M.; Alijani, M.; Motola, M.; Hromadko, L.; Macak, J. M. Intrinsic Properties of Anodic TiO_2 Nanotube Layers: In-Situ XRD Annealing of TiO_2 Nanotube Layers. *Ceram. Int.* **2023**, *49* (14), 24293−24301.
(30) Jaeger, V.; Wilson, W.; Subramanian, V. R. Photodegradation of Methyl Orange and 2,3-Butanedione on Titanium-Dioxide Nanotube Arrays Efficiently Synthesized on Titanium Coils. *Appl. Catal., B* **2011**, *110*, 6−13.
(31) Nischk, M.; Mazierski, P.; Gazda, M.; Zaleska, A. Ordered TiO_2 Nanotubes: The Effect of Preparation Parameters on the Photocatalytic Activity in Air Purification Process. *Appl. Catal., B* **2014**, *144*, 674−685.
(32) Sopha, H.; Baudys, M.; Hromadko, L.; Lhotka, M.; Pavlinak, D.; Krysa, J.; Macak, J. M. Scaling up Anodic TiO_2 Nanotube Layers − Influence of the Nanotube Layer Thickness on the Photocatalytic Degradation of Hexane and Benzene. *Appl. Mater. Today* **2022**, *29*, No. 101567.
(33) Kontos, A. G.; Katsanaki, A.; Likodimos, V.; Maggos, T.; Kim, D.; Vasilakos, C.; Dionysiou, D. D.; Schmuki, P.; Falaras, P. Continuous Flow Photocatalytic Oxidation of Nitrogen Oxides over Anodized Nanotubular Titania Films. *Chem. Eng. J.* **2012**, *179*, 151−157.
(34) Lincho, J.; Gomes, J.; Kobylanski, M.; Bajorowicz, B.; Zaleska-Medynska, A.; Martins, R. C. TiO_2 Nanotube Catalysts for Parabens Mixture Degradation by Photocatalysis and Ozone-Based Technologies. *Process Saf. Environ. Prot.* **2021**, *152*, 601−613.
(35) Mena, E.; Martín de Vidales, M. J.; Mesones, S.; Marugán, J. Influence of Anodization Mode on the Morphology and Photocatalytic Activity of TiO_2-NTs Array Large Size Electrodes. *Catal. Today* **2018**, *313*, 33−39.
(36) Xiang, C.; Sun, L.; Wang, Y.; Wang, G.; Zhao, X.; Zhang, S. Large-Scale, Uniform, and Superhydrophobic Titania Nanotubes at the Inner Surface of 1000 mm Long Titanium Tubes. *J. Phys. Chem. C* **2017**, *121* (28), 15448−15455.
(37) Kim, H.; Kim, D.; Kim, W.; Ha, Y.-C.; Sim, S.-J.; Kim, S.; Choi, W. Anodic TiO_2 Nanotube Layer Directly Formed on the Inner Surface of Ti Pipe for a Tubular Photocatalytic Reactor. *Appl. Catal., A* **2016**, *521* (1), 174−181.
(38) Motola, M.; Baudys, M.; Zazpe, R.; Krbal, M.; Michalička, J.; Rodriguez-Pereira, J.; Pavliňák, D.; Přikryl, J.; Hromádko, L.; Sopha, H.; Krýsa, J.; Macak, J. M. 2D MoS_2 Nanosheets on 1D Anodic TiO_2 Nanotube Layers: An Efficient Co-Catalyst for Liquid and Gas Phase Photocatalysis. *Nanoscale* **2019**, *11* (48), 23126−23131.
(39) Motola, M.; Satrapinsky, L.; Roch, T.; Jan, Š.; Kupčík, J.; Klementová, M.; Jakubičková, M.; Peterka, F.; Plesch, G. Anatase TiO_2 Nanotube Arrays and Titania Films on Titanium Mesh for Photocatalytic NO_X Removal and Water Cleaning. *Catal. Today* **2017**, *287*, 59−64.
(40) Sopha, H.; Kashimbetova, A.; Hromadko, L.; Saldan, I.; Celko, L.; Montufar, E. B.; Macak, J. M. Anodic TiO_2 Nanotubes on 3D-Printed Titanium Meshes for Photocatalytic Applications. *Nano Lett.* **2021**, *21* (20), 8701−8706.
(41) Sato, N. A Theory for Breakdown of Anodic Oxide Films on Metals. *Electrochim. Acta* **1971**, *16*, 1683−1692.
(42) Liang, H.; Li, X. Effects of Structure of Anodic TiO_2 Nanotube Arrays on Photocatalytic Activity for the Degradation of 2,3-Dichlorophenol in Aqueous Solution. *J. Hazard. Mater.* **2009**, *162* (2−3), 1415−1422.
(43) Sreekantan, S.; Hazan, R.; Lockman, Z. Photoactivity of Anatase-Rutile TiO_2 Nanotubes Formed by Anodization Method. *Thin Solid Films* **2009**, *518* (1), 16−21.
(44) Fang, D.; Luo, Z.; Huang, K.; Lagoudas, D. C. Effect of Heat Treatment on Morphology, Crystalline Structure and Photocatalysis Properties of TiO_2 Nanotubes on Ti Substrate and Freestanding Membrane. *Appl. Surf. Sci.* **2011**, *257* (15), 6451−6461.
(45) Moriai, K.; Nakajima, N.; Moriyoshi, C.; Maruyama, H. Synthesis of TiO_2 Nanotubes: Effect of Post-Treatment on Crystallinity and Photocatalytic Activity. *Mater. Res. Express* **2017**, *4* (4), No. 045017.
(46) Viet, P. Van; Phuong Trang, D. D.; Phat, B. D.; Hieu, L. Van; Thi, C. M. Understanding the Effect of Annealing Temperature on Crystalline Structure, Morphology, and Photocatalytic Activity of Silver-Loaded TiO_2 Nanotubes. *Superlattices Microstruct.* **2018**, *117*, 305−316.
(47) Perillo, P. M.; Rodríguez, D. F. Photocatalysis of Methyl Orange Using Free Standing TiO_2 Nanotubes under Solar Light. *Environ. Nanotechnol., Monit. Manage.* **2021**, *16* (April), 100479.
(48) Sebek, M.; Peppel, T.; Lund, H.; Medic, I.; Springer, A.; Mazierski, P.; Zaleska-Medynska, A.; Strunk, J.; Steinfeldt, N. Thermal Annealing of Ordered TiO_2 Nanotube Arrays with Water Vapor-Assisted Crystallization under a Continuous Gas Flow for Superior Photocatalytic Performance. *Chem. Eng. J.* **2021**, *425* (May), No. 130619.
(49) Das, S.; Zazpe, R.; Prikryl, J.; Knotek, P.; Krbal, M.; Sopha, H.; Podzemna, V.; Macak, J. M. Influence of Annealing Temperatures on the Properties of Low Aspect-Ratio TiO_2 Nanotube Layers. *Electrochim. Acta* **2016**, *213*, 452−459.
(50) Jarosz, M.; Syrek, K.; Kapusta-Kołodziej, J.; Mech, J.; Małek, K.; Hnida, K.; Łojewski, T.; Jaskuła, M.; Sulka, G. D. Heat Treatment Effect on Crystalline Structure and Photoelectrochemical Properties of Anodic TiO_2 Nanotube Arrays Formed in Ethylene Glycol and Glycerol Based Electrolytes. *J. Phys. Chem. C* **2015**, *119* (42), 24182−24191.
(51) Bickley, R. I.; Gonzalez-Carreno, T.; Lees, J. S.; Palmisano, L.; Tilley, R. J. D. A Structural Investigation of Titanium Dioxide photocatalysts. *J. Solid State Chem.* **1991**, *92* (1), 178−190.
(52) Vranješ, M.; Šaponjić, Z. V.; Živković, L. S.; Despotović, V. N.; Šojić, D. V.; Abramović, B. F.; Čomor, M. I. Elongated Titania nanostructures as Efficient photocatalysts for Degradation of Selected Herbicides. *Appl. Catal., B* **2014**, *160−161* (1), 589−596.
(53) Pfeifer, V.; Erhart, P.; Li, S.; Rachut, K.; Morasch, J.; Brötz, J.; Reckers, P.; Mayer, T.; Rühle, S.; Zaban, A.; Mora Seró, I.; Bisquert, J.; Jaegermann, W.; Klein, A. Energy Band Alignment between Anatase and Rutile TiO_2. *J. Phys. Chem. Lett.* **2013**, *4* (23), 4182−4187.
(54) Hurum, D. C.; Agrios, A. G.; Gray, K. A.; Rajh, T.; Thurnauer, M. C. Explaining the Enhanced Photocatalytic Activity of Degussa P25 Mixed-Phase TiO_2 Using EPR. *J. Phys. Chem. B* **2003**, *107* (19), 4545−4549.
(55) Deák, P.; Aradi, B.; Frauenheim, T. Band Lineup and Charge Carrier Separation in Mixed Rutile-Anatase Systems. *J. Phys. Chem. C* **2011**, *115* (8), 3443−3446.
(56) Scanlon, D. O.; Dunnill, C. W.; Buckeridge, J.; Shevlin, S. A.; Logsdail, A. J.; Woodley, S. M.; Catlow, C. R. A.; Powell, M. J.; Palgrave, R. G.; Parkin, I. P.; Watson, G. W.; Keal, T. W.; Sherwood, P.; Walsh, A.; Sokol, A. A. Band Alignment of Rutile and Anatase TiO_2. *Nat. Mater.* **2013**, *12* (9), 798−801.
(57) Sepúlveda, M.; Saldan, I.; Mahnaz, A.; Cicmancova, V.; Michalicka, J.; Hromadko, L.; Bulánek, R.; Sopha, H.; Macak, J. M. Magnetically Guidable Single TiO_2 Nanotube photocatalyst: Structure and Photocatalytic Properties. *Ceram. Int.* **2023**, *49* (4), 6764−6771.
(58) Baudys, M.; Berthet, E.; Macak, J. M.; Lhotka, M.; Krýsa, J. Photocatalytic Degradation of Gaseous Pollutants on Nanostructured TiO_2 Films of Various Thickness and Surface Area. *Photochem. Photobiol. Sci.* **2023**, *22* (4), 883−892.

https://doi.org/10.1021/acsanm.3c03199
ACS Appl. Nano Mater. 2023, 6, 17053−17059